

Electron Transport along Screw Dislocations in a Strong Topological Insulator

Tatsuro Sakaguchi and Yositake Takane

*Graduate School of Advanced Science and Engineering,
Hiroshima University, Higashihiroshima, Hiroshima 739-8530, Japan*

(Received)

In a three-dimensional strong topological insulator, gapless helical surface states appear everywhere on its surface. In the presence of a screw dislocation, gapless helical modes also appear in the vicinity of the corresponding dislocation line. Let us focus on a case where a pair of screw dislocations connects the top and bottom surfaces of a strong topological insulator with a shape of rectangular parallelepiped. The dislocation-induced helical modes are expected to act as one-dimensional conduction channels connecting the top and bottom surfaces. To examine this expectation, we calculate the two-terminal conductance between a pair of electrodes placed on the top and bottom surfaces. We found that the dislocation-induced helical modes and the helical surface states on the side surface contribute to the two-terminal conductance. The contribution of the dislocation-induced helical modes becomes more dominant than that of the helical surface states in certain situations.

1. Introduction

Three-dimensional \mathbb{Z}_2 topological insulators are characterized by strong and weak indices $(\nu_0, \nu_x, \nu_y, \nu_z)$.¹⁻⁴ A strong topological insulator with $\nu_0 = 1$ hosts gapless topological boundary states everywhere on its surface. These two-dimensional states, which are protected by time-reversal symmetry, are helical because they exhibit helical spin texture, i.e., the spin orientation of a surface state is tied to its momentum. This helical nature of gapless surface states also manifests itself in topological states induced by lattice defects. When a screw or edge dislocation is inserted into a strong topological insulator, a pair of counterpropagating gapless modes appears in the vicinity of the corresponding dislocation line under a certain condition [see Eq. (17)].^{5,6} These one-dimensional modes are also helical in that the spin orientation of a one-dimensional state determines its propagating direction, i.e., if the gapless mode propagating in one direction consists of spin-up states, that propagating in the other direction consists of spin-down states. The appearance of one-dimensional gapless modes due to the insertion of a screw or edge dislocation has also been demonstrated not only in gapped topological systems⁷⁻¹² but also in Weyl and Dirac semimetals.¹³⁻²⁰

For definiteness, let us consider a \mathbb{Z}_2 topological insulator of rectangular parallelepiped shape into which a pair of screw dislocations is inserted [see Fig. 1(a)]. We assume that the screw dislocations are parallel to the z -axis and connect the top and bottom surfaces of the system. A step edge is induced on the top and bottom surfaces because of the presence of the screw dislocations [see Fig. 1(b)]. In the weak topological insulator case of $\nu_0 = 0$, we can set up the system such that a pair of counterpropagating helical modes appears along the loop consisting of two dislocation lines and two step edges.⁹ In this setup, helical surface states appear only on the side surface without penetrating the top and bottom surfaces. Therefore, the one-dimensional helical modes are isolated

from the helical surface states. In the strong topological insulator case of $\nu_0 = 1$, helical surface states appear on all surfaces. Hence, the one-dimensional helical modes are hybridized with the helical surface states on the top and bottom surfaces near the step edges. In the presence of such hybridization, we expect that the one-dimensional helical modes along each dislocation line act as conduction channels connecting the top and bottom surfaces.^{21,22}

We examine whether the dislocation-induced helical modes act as conduction channels for electron transport. A simple way to do this is to calculate the two-terminal conductance \mathcal{G} between two electrodes one of which is placed on the top surface and the other one is placed on the bottom surface. The dislocation-induced helical modes hybridized with the helical surface states contribute to \mathcal{G} . However, they are not the only channels connecting the two electrodes. Because the helical surface states themselves directly connect the electrodes through the side surface, they also contribute to \mathcal{G} . In contrast, the contribution of bulk states is negligible if the Fermi energy is in the subgap region of the strong topological insulator. Thus, \mathcal{G} is governed by the dislocation-induced helical modes and the helical surface states. We must separate these two contributions to examine the role of the dislocation-induced helical modes.

In this paper, we calculate the two-terminal conductance \mathcal{G} between a pair of electrodes placed on the top and bottom surfaces of a strong topological insulator with a shape of rectangular parallelepiped. We found that the dislocation-induced helical modes dominantly contribute to \mathcal{G} when the helical surface states on the side surface are eliminated by imposing a periodic boundary condition in the x - and y -directions. If the helical surface states on the side surface are considered under an open boundary condition in the x - and y -directions, the contribution of the dislocation-induced helical modes does not dominate that of the helical surface states. However, the

former contribution dominates the latter contribution if the area of the top and bottom surfaces is increased while keeping the areal density of the dislocation pairs constant. We also found that the dislocation-induced helical modes become dominant if an energy gap is opened in the spectrum of the helical surface states on the side surface by applying a local perturbation that breaks the time-reversal symmetry.

In the next section, we introduce a tight-binding Hamiltonian for a \mathbb{Z}_2 topological insulator. In Sect. 3, we briefly describe the method for calculating the two-terminal conductance \mathcal{G} between two electrodes. In Sect. 4, we provide the numerical results of \mathcal{G} for two cases: a case without the side surface under a periodic boundary condition in the x - and y -directions, and a case with the side surface under an open boundary condition in the x - and y -directions. The last section is devoted to a summary and short discussion.

2. Model

We introduce a tight-binding model for a \mathbb{Z}_2 topological insulator on a cubic lattice with a lattice constant a in a rectangular parallelepiped shape of volume $N_x \times N_y \times N_z$. The indices l , m , and n are used to specify lattice sites in the x -, y -, and z -directions, respectively, where $1 \leq l \leq N_x$, $1 \leq m \leq N_y$, and $1 \leq n \leq N_z$. The four-component state vector for the (l, m, n) th site is expressed as

$$|l, m, n\rangle = \left[|l, m, n\rangle_{1\uparrow} |l, m, n\rangle_{2\uparrow} |l, m, n\rangle_{1\downarrow} |l, m, n\rangle_{2\downarrow} \right], \quad (1)$$

where each lattice site has orbital and spin degrees of freedom described by $\eta = 1, 2$ and $\sigma = \uparrow, \downarrow$, respectively. The Hamiltonian is given by $H = H_d + H_x + H_y + H_z$ with²³⁾

$$H_d = \sum_{l=1}^{N_x} \sum_{m=1}^{N_y} \sum_{n=1}^{N_z} |l, m, n\rangle \mathcal{H}_d \langle l, m, n|, \quad (2)$$

$$H_x = \sum_{l=1}^{N_x-1} \sum_{m=1}^{N_y} \sum_{n=1}^{N_z} |l+1, m, n\rangle \mathcal{H}_x \langle l, m, n| + \text{h.c.}, \quad (3)$$

$$H_y = \sum_{l=1}^{N_x} \sum_{m=1}^{N_y-1} \sum_{n=1}^{N_z} |l, m+1, n\rangle \mathcal{H}_y \langle l, m, n| + \text{h.c.}, \quad (4)$$

$$H_z = \sum_{l=1}^{N_x} \sum_{m=1}^{N_y} \sum_{n=1}^{N_z-1} |l, m, n+1\rangle \mathcal{H}_z \langle l, m, n| + \text{h.c.}, \quad (5)$$

where

$$\mathcal{H}_d = \begin{bmatrix} M\tau_z & 0_{2 \times 2} \\ 0_{2 \times 2} & M\tau_z \end{bmatrix}, \quad (6)$$

$$\mathcal{H}_x = \begin{bmatrix} -m_{\parallel}\tau_z & \frac{i}{2}A\tau_x \\ \frac{i}{2}A\tau_x & -m_{\parallel}\tau_z \end{bmatrix}, \quad (7)$$

$$\mathcal{H}_y = \begin{bmatrix} -m_{\parallel}\tau_z & \frac{1}{2}A\tau_x \\ -\frac{1}{2}A\tau_x & -m_{\parallel}\tau_z \end{bmatrix}, \quad (8)$$

$$\mathcal{H}_z = \begin{bmatrix} -m_{\perp}\tau_z + \frac{i}{2}B\tau_x & 0_{2 \times 2} \\ 0_{2 \times 2} & -m_{\perp}\tau_z - \frac{i}{2}B\tau_x \end{bmatrix}. \quad (9)$$

Here, M is given by

$$M = m_0 + 4m_{\parallel} + 2m_{\perp}, \quad (10)$$

and τ_q is the q -component of Pauli matrices ($q \in x, y$, and z). The strong and weak indices $(\nu_0, \nu_x \nu_y \nu_z)$ characterizing a \mathbb{Z}_2 topological insulator are determined by the parameters m_0 , m_{\parallel} , and m_{\perp} . We set $m_{\perp}/m_{\parallel} = 1$ and $m_0/m_{\parallel} = -10$ throughout this paper. With this setting, the Hamiltonian H describes the strong topological insulator with $(\nu_0, \nu_x \nu_y \nu_z) = (1, 111)$.²⁴⁾

The Hamiltonian, consisting of the four terms specified in Eqs. (2)–(5), describes a system under an open boundary condition in the x -, y -, and z -directions. In addition to the system under the open boundary condition in the three directions, a system under a periodic boundary condition in the x - and y -directions (see Sect. 4) is also considered to eliminate the helical surface states on the side surface. The periodic boundary condition in the two directions is implemented if the following boundary terms are added to H :

$$\Delta H_x = \sum_{m=1}^{N_y} \sum_{n=1}^{N_z} |1, m, n\rangle \mathcal{H}_x \langle N_x, m, n| + \text{h.c.}, \quad (11)$$

$$\Delta H_y = \sum_{l=1}^{N_x} \sum_{n=1}^{N_z} |l, 1, n\rangle \mathcal{H}_y \langle l, N_y, n| + \text{h.c.} \quad (12)$$

The bulk spectrum of this model is given as $E(\mathbf{k}) = \pm \sqrt{\Xi(\mathbf{k})}$ in the infinite volume limit, where $\mathbf{k} = (k_x, k_y, k_z)$ is a wave vector and

$$\Xi(\mathbf{k}) = [M - 2m_{\parallel}(\cos(k_x a) + \cos(k_y a)) - 2m_{\perp} \cos(k_z a)]^2 + A^2(\sin^2(k_x a) + \sin^2(k_y a)) + B^2 \sin^2(k_z a). \quad (13)$$

In the case where $m_{\perp}/m_{\parallel} = 1$ and $m_0/m_{\parallel} = -10$, the energy gap defined as $E_g = \min_{\mathbf{k}} \{\sqrt{\Xi(\mathbf{k})}\}$ is given by $E_g/m_{\parallel} = 2$.

Then, let us introduce a pair of screw dislocations parallel to the z -axis in our tight-binding model without deforming the lattice structure itself. We assume that the screw dislocations are centered at $(x_{1D}, y_D) = a(l_{1D} + \frac{1}{2}, m_D + \frac{1}{2})$ and $(x_{2D}, y_D) = a(l_{2D} + \frac{1}{2}, m_D + \frac{1}{2})$ with

$$l_{1D} = \frac{N_x}{4}, \quad l_{2D} = \frac{3N_x}{4}, \quad m_D = \frac{N_y}{2}, \quad (14)$$

where the origin of the x - and y -coordinates $(x, y) = (0, 0)$ is set at $(l, m) = (0, 0)$. Here, it is implicitly assumed that N_x and N_y are integers that are multiple of 4 and 2, respectively. We also assume that the screw dislocations at (x_{1D}, y_D) and (x_{2D}, y_D) have a displacement of N unit atomic layers, and they are characterized by the Burgers vectors $\mathbf{b}_1 = (0, 0, N)$ and $\mathbf{b}_2 = (0, 0, -N)$, respectively. Let us consider a slip plane with its two edges identical to dislocation lines [see Fig. 1(a)] and modify the hopping terms in H across it so that each term connects two different layers in the z -direction [see Fig. 1(b)].^{8,13)} To do this, we reconnect the hopping terms in H_y in the region of $l_{1D} + 1 \leq l \leq l_{2D}$ by performing the following replacement:

$$|l, m_D + 1, n\rangle \mathcal{H}_y \langle l, m_D, n| + \text{h.c.}$$

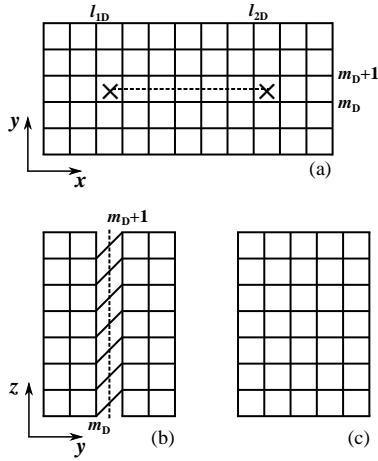


Fig. 1. Lattice system with a pair of screw dislocations with a displacement of one unit atomic layer (i.e., $N = 1$), where each solid line between two neighboring sites represents a hopping term in H_x , H_y , or H_z that directly connects the two sites. The dotted lines represent the slip plane across which the hopping terms in H are modified. (a) Top view with the crosses representing the dislocation centers. (b) Side view of the modified region of $l_{1D} + 1 \leq l \leq l_{2D}$. A step edge of one unit atomic layer is induced by the screw dislocations at $m = m_D$ on the top surface and at $m = m_D + 1$ on the bottom surface. (c) Side view of the unmodified region of $l \leq l_{1D}$ or $l_{2D} + 1 \leq l$.

$$\rightarrow |l, m_D + 1, n + N\rangle \mathcal{H}_y \langle l, m_D, n| + \text{h.c.}, \quad (15)$$

which shows that the site with $m = m_D$ on the n th layer is connected to the site with $m = m_D + 1$ on the $n + N$ th layer across the slip plane. Consequently, H_y becomes

$$\begin{aligned} H_y &= \sum_{l=1}^{N_x} \sum_{\substack{m=1 \\ (m \neq m_D)}}^{N_y-1} \sum_{n=1}^{N_z} |l, m + 1, n\rangle \mathcal{H}_y \langle l, m, n| + \text{h.c.} \\ &+ \sum_{l=1}^{l_{1D}} \sum_{n=1}^{N_z} |l, m_D + 1, n\rangle \mathcal{H}_y \langle l, m_D, n| + \text{h.c.} \\ &+ \sum_{l=l_{1D}+1}^{l_{2D}} \sum_{n=1}^{N_z-N} |l, m_D + 1, n + N\rangle \mathcal{H}_y \langle l, m_D, n| + \text{h.c.} \\ &+ \sum_{l=l_{2D}+1}^{N_x} \sum_{n=1}^{N_z} |l, m_D + 1, n\rangle \mathcal{H}_y \langle l, m_D, n| + \text{h.c.} \quad (16) \end{aligned}$$

after the replacement. A step edge with a length of $a(l_{2D} - l_{1D})$ is induced by the screw dislocations on the top and bottom surfaces [see Fig. 1(b)].

As shown in Ref. 5, the appearance of one-dimensional gapless helical modes confined in the vicinity of a screw dislocation is determined by the Burgers vector \mathbf{b} characterizing the screw dislocation and the vector \mathbf{M} defined in terms of the weak indices as $\mathbf{M} = (\nu_x, \nu_y, \nu_z)$. The gapless helical modes appear if and only if

$$\mathbf{b} \cdot \mathbf{M} = 1 \pmod{2}. \quad (17)$$

In our setting, $\mathbf{M} = (1, 1, 1)$ and $\mathbf{b}_1 = -\mathbf{b}_2 = (0, 0, N)$; thus, the helical modes appear in our system when N is an odd integer.

3. Simulation of Electron Transport

We study electron transport at zero temperature between the top and bottom surfaces of a strong topological insulator in the presence or absence of a pair of screw dislocations parallel to the z -axis. To characterize electron transport, we calculate the two-terminal conductance between two electrodes, where the first electrode is placed on the top surface and the second one is placed on the bottom surface. For simplicity, we assume that each electrode is coupled with the top or bottom surface of the strong topological insulator in a rectangular region with 5 sites in the x -direction and 4 sites in the y -direction. Hereafter, we use $\mathbf{r} \equiv (l, m, n)$ to denote the position of each site in the system. The rectangular region on the top surface and that on the bottom surface are specified by $\mathbf{r}_1 = (l, m, N_z)$ and $\mathbf{r}_2 = (l, m, 1)$, respectively, with $l_C - 2 \leq l \leq l_C + 2$ and $m_C - 1 \leq m \leq m_C + 2$.

We calculate the two-terminal conductance between two electrodes using a formula in terms of Green's function.^{25,26} Let us define Green's function as

$$G = (E_F \mathbf{1} - H - \Sigma)^{-1}, \quad (18)$$

where $\mathbf{1} = \sum_{\mathbf{r}} |\mathbf{r}\rangle \langle \mathbf{r}|$, E_F is the Fermi energy, and Σ is the self-energy describing the coupling of the system with the electrodes. Here, $|\mathbf{r}\rangle$ represents $|l, m, n\rangle$. We assume that $\Sigma = \Sigma_1 + \Sigma_2$, with

$$\Sigma_1 = -i\gamma \sum_{\mathbf{r} \in S_1} |\mathbf{r}\rangle \langle \mathbf{r}|, \quad (19)$$

$$\Sigma_2 = -i\gamma \sum_{\mathbf{r} \in S_2} |\mathbf{r}\rangle \langle \mathbf{r}|, \quad (20)$$

where γ is the coupling strength and S_p denotes the set of 5×4 sites in contact with the p th electrode ($p = 1, 2$). In terms of Green's function, the transmission function from the bottom electrode to the top electrode is defined as²⁵)

$$T = \text{Tr} \{ \Gamma_1 G \Gamma_2 G^\dagger \}, \quad (21)$$

where $\Gamma_p \equiv i(\Sigma_p - \Sigma_p^\dagger)$. The two-terminal conductance \mathcal{G} between the top and bottom electrodes is expressed as

$$\mathcal{G} = \frac{e^2}{h} T. \quad (22)$$

In addition to $m_\perp/m_\parallel = 1$ and $m_0/m_\parallel = -10$, the following parameters are used: $A/m_\parallel = 1.5$, $B/m_\parallel = 2.0$, and $\gamma/m_\parallel = 0.2$.

4. Numerical Results

In this section, we consider the transmission function T instead of the two-terminal conductance \mathcal{G} . We numerically calculate T in the presence and absence of the screw dislocations in the cases with and without the side surface. The system size is fixed as $N_x = 80$, $N_y = 40$, and $N_z = 52$. The locations of the two electrodes are specified by $l_C = 20$ and $m_C = 10$. The screw dislocations are assumed to have a displacement of one unit atomic layer (i.e., $N = 1$) unless otherwise noted.

Let us first consider the case without the side surface under the periodic boundary condition in the x - and y -directions. Figure 2 shows the numerical results of T in

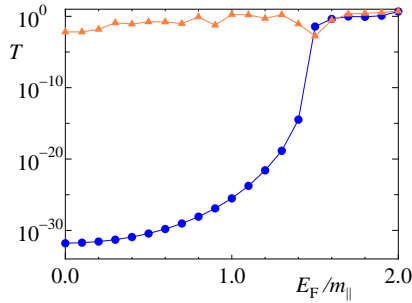


Fig. 2. (Color online) Numerical results of T in the presence of the screw dislocations with $N = 1$ (triangles) and in the absence of the screw dislocations (circles) for several values of E_F/m_{\parallel} under the periodic boundary condition in the x - and y -directions. The solid lines serve as visual guides.

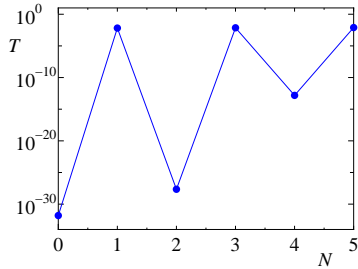


Fig. 3. (Color online) Numerical results of T at $E_F/m_{\parallel} = 0.0$ for $N = 0, 1, 2, 3, 4,$ and 5 . Although the values of T for $N = 1, 3,$ and 5 may look identical, they are slightly different from each other. The solid line serves as a visual guide.

the presence and absence of the screw dislocations for various values of E_F in the range of $0 \leq E_F/m_{\parallel} \leq 2$. We observe that T in the presence of the screw dislocations is orders of magnitude larger than that in the absence of the screw dislocations when E_F/m_{\parallel} is small, showing that the dislocation-induced helical modes certainly contribute to T . The quantitative difference between the two cases becomes small as E_F/m_{\parallel} increases and almost vanishes when $E_F/m_{\parallel} \gtrsim 1.6$. This behavior is ascribed to the fact that the contribution of the bulk states to T , which is almost independent of the presence or absence of the screw dislocations, increases rapidly as E_F approaches the gap edge. Figure 2 indicates that $E_F/m_{\parallel} = 1.6$ corresponds to the gap edge.²⁷⁾

Recall that our setting of $m_{\perp}/m_{\parallel} = 1$ and $m_0/m_{\parallel} = -10$ results in $(\nu_0, \nu_x \nu_y \nu_z) = (1, 111)$. As noted in Sect. 2, the dislocation-induced helical modes appear in our system when N is an odd integer. To observe how N affects T , we numerically calculate T in the presence of the screw dislocations at $E_F/m_{\parallel} = 0.0$ for $N = 0, 1, 2, 3, 4,$ and 5 , where $N = 0$ corresponds to the case in the absence of the screw dislocations. The numerical results shown in Fig. 3 indicate that T using an odd N is orders of magnitude larger than that using an even N . This confirms the theoretical expectation.

Next, we consider the case with the side surface under the open boundary condition in the x - and y -directions to elucidate the effect of the helical surface states as conduc-

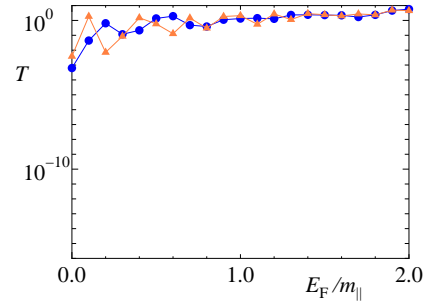


Fig. 4. (Color online) Numerical results of T in the presence of the screw dislocations with $N = 1$ (triangles) and in the absence of the screw dislocations (circles) for several values of E_F/m_{\parallel} under the open boundary condition in the x - and y -directions. The solid lines serve as visual guides.

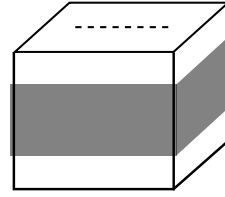


Fig. 5. Schematic of the system with its side surface partly covered with an insulating ferromagnetic layer. The dashed line on the top surface represents the step edge connecting two dislocation lines.

tion channels connecting two electrodes. Figure 4 shows the numerical results of T in the presence and absence of the screw dislocations for various values of E_F in the range of $0 \leq E_F/m_{\parallel} \leq 2$. We observe that the values of T in the presence and absence of the screw dislocations are of the same order of magnitude, indicating that the contribution of the dislocation-induced helical modes to T is the same order of magnitude as, or smaller than, that of the helical surface states. This is because only one pair of screw dislocations is present in our setup. Let us consider a situation in which many pairs of screw dislocations are present in the system. If the areal density of the dislocation pairs is kept constant, the contribution of the dislocation-induced helical modes to T is proportional to $N_x \times N_y$, whereas that of the helical surface states is roughly proportional to $N_x + N_y$. Therefore, the contribution of the dislocation-induced helical modes to T is dominated by that of the helical surface states when both N_x and N_y are very small as in our setup. Conversely, the contribution of the dislocation-induced helical modes becomes much larger than that of the helical surface states if both N_x and N_y are increased while keeping the areal density of the dislocation pairs constant.

Here, we briefly comment on the fluctuation in T with the change in E_F/m_{\parallel} . This is mainly ascribed to finite size effects, which result in the quantization of eigenstates. Indeed, the fluctuation is large near $E_F/m_{\parallel} = 0$ where quantization is particularly notable.

Finally, we show that, even in the case with the side surface with small N_x and N_y , the dislocation-induced helical modes can dominantly contribute to T . This is

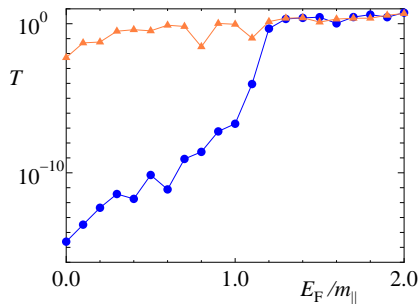


Fig. 6. (Color online) Numerical results of T in the presence of the screw dislocations with $N = 1$ (triangles) and in the absence of the screw dislocations (circles) when $m_{\text{mag}}/m_{\parallel} = 1.2$ for several values of E_F/m_{\parallel} under the open boundary condition in the x - and y -directions. The solid lines serve as visual guides.

realized if an energy gap is opened in the spectrum of the helical surface states on the side surface, resulting in the blockade of the conduction channels through the helical surface states. We introduce the energy gap by attaching surface magnetization to every site on the side surface in the region of $n_1 + 1 \leq n \leq n_2$, where $n_1 = N_z/4$ and $n_2 = 3N_z/4$. This can be implemented by surrounding the sample with an insulating ferromagnetic layer (see Fig. 5) such that its magnetization is everywhere normal to the surface.^{28, 29)} The perturbation is expressed as

$$H_{\text{mag}} = \sum'_{l,m} \sum_{n=n_1+1}^{n_2} |l, m, n\rangle \mathcal{H}_{\text{mag}} |l, m, n\rangle \quad (23)$$

with

$$\mathcal{H}_{\text{mag}} = m_{\text{mag}} \sigma_{\perp}(l, m) \otimes \tau_0, \quad (24)$$

where τ_0 is a 2×2 unit matrix and the summation over l and m is restricted to sites in the outermost layer of the side surface. Here, $\sigma_{\perp}(l, m)$ is given as

$$\sigma_{\perp}(l, m) = \begin{cases} -\sigma_x & (l = 1, 2 \leq m \leq N_y - 1), \\ \sigma_x & (l = N_x, 2 \leq m \leq N_y - 1), \\ -\sigma_y & (2 \leq l \leq N_x - 1, m = 1), \\ \sigma_y & (2 \leq l \leq N_x - 1, m = N_y) \end{cases} \quad (25)$$

except in the sites on the four corners, where it is given as

$$\sigma_{\perp}(l, m) = \begin{cases} \frac{1}{\sqrt{2}}(-\sigma_x - \sigma_y) & (l = 1, m = 1), \\ \frac{1}{\sqrt{2}}(-\sigma_x + \sigma_y) & (l = 1, m = N_y), \\ \frac{1}{\sqrt{2}}(\sigma_x - \sigma_y) & (l = N_x, m = 1), \\ \frac{1}{\sqrt{2}}(\sigma_x + \sigma_y) & (l = N_x, m = N_y). \end{cases} \quad (26)$$

Figure 6 shows the numerical results of T in the presence and absence of the screw dislocations when $m_{\text{mag}}/m_{\parallel} = 1.2$ for various values of E_F in the range of $0 \leq E_F/m_{\parallel} \leq 2$. We observe that T in the presence of the screw dislocations is orders of magnitude larger than that in the absence of the screw dislocations when E_F/m_{\parallel} is small. By comparing the results when $m_{\text{mag}}/m_{\parallel} = 0$ (Fig. 4) and those when $m_{\text{mag}}/m_{\parallel} = 1.2$ (Fig. 6), we found that T in the presence of the screw dislocations is almost unaffected by m_{mag} . In contrast, T in the absence of the screw

dislocations strongly reduces when $m_{\text{mag}}/m_{\parallel} = 1.2$. The reduction in T in the absence of the screw dislocations can be ascribed to the blockade of the conduction channels through the helical surface states due to the energy gap induced by surface magnetization.³⁰⁾ The insensitivity of T to m_{mag} in the presence of the screw dislocations indicates that the conduction channels along the screw dislocations are unaffected by surface magnetization. The results show that the contribution of the dislocation-induced helical modes to T becomes more dominant than that of the helical surface states if an energy gap is opened in the spectrum of the helical surface states on the side surface.

5. Summary and Short Discussion

If screw dislocations are inserted into a strong topological insulator, one-dimensional helical modes appear along each screw dislocation under a certain condition. To determine whether the dislocation-induced helical modes act as one-dimensional conduction channels, we calculate the two-terminal conductance \mathcal{G} between a pair of electrodes placed on the top and bottom surfaces of a strong topological insulator, into which a pair of screw dislocations is inserted such that it connects the top and bottom surfaces. From the results of \mathcal{G} , we conclude that the dislocation-induced helical modes certainly act as one-dimensional conduction channels connecting the top and bottom surfaces.

Our conclusion is consistent with the results of experimental studies,^{21, 22)} in which the conductivity in the presence of high-density dislocations is enhanced in the direction parallel to the dislocations. Unfortunately, a detailed comparison between our numerical results and the experimental results is difficult. The main reason for this is that our model system with only one pair of screw dislocations is considerably smaller than the experimental systems with high-density dislocations. Another reason is that our tight-binding model cannot describe a realistic feature of the experimental systems. Indeed, in contrast to the fact that the contribution of helical surface states to the conductivity is less dominant than that of bulk states in the experiment reported in Ref. 21, the former is much more dominant than the latter in our model as long as the Fermi energy is in the subgap region.

Acknowledgment

This work was supported by JSPS KAKENHI Grant Number JP21K03405.

- 1) L. Fu, C. L. Kane, and E. J. Mele, Phys. Rev. Lett. **98**, 106803 (2007).
- 2) J. E. Moore and L. Balents, Phys. Rev. B **75**, 121306 (2007).
- 3) R. Roy, Phys. Rev. B **79**, 195322 (2009).
- 4) M. Z. Hasan and C. L. Kane, Rev. Mod. Phys. **82**, 3045 (2010).
- 5) Y. Ran, Y. Zhang, and A. Vishwanath, Nat. Phys. **5**, 298 (2009).
- 6) Y. Zhang, Y. Ran, and A. Vishwanath, Phys. Rev. B **79**, 245331 (2009).
- 7) J. C. Y. Teo and C. L. Kane, Phys. Rev. B **82**, 115120 (2010).
- 8) K.-I. Imura, Y. Takane, and A. Tanaka, Phys. Rev. B **84**, 035443 (2011).

- 9) Y. Yoshimura, A. Matsumoto, Y. Takane, and K.-I. Imura, *Phys. Rev. B* **88**, 045408 (2013).
- 10) K. Shiozaki and M. Sato, *Phys. Rev. B* **90**, 165114 (2014).
- 11) R.-J. Slager, A. Mesaros, V. Juričić, and J. Zaanen, *Phys. Rev. B* **90**, 241403 (2014).
- 12) C. Pauly, B. Rasche, K. Koepf, M. Liebmann, M. Pratzner, M. Richter, J. Kellner, M. Eschbach, B. Kaufmann, L. Plucinski, C. M. Schneider, M. Ruck, J. van den Brink, and M. Morgenstern, *Nat. Phys.* **11**, 338 (2015).
- 13) K.-I. Imura and Y. Takane, *Phys. Rev. B* **84**, 245415 (2011).
- 14) H. Sumiyoshi and S. Fujimoto, *Phys. Rev. Lett.* **116**, 166601 (2016).
- 15) M. N. Chernodub and M. A. Zubkov, *Phys. Rev. B* **95**, 115410 (2017).
- 16) K. Kodama and Y. Takane, *J. Phys. Soc. Jpn.* **88**, 054715 (2019).
- 17) Z.-M. Huang, L. Li, J. Zhou, and H.-H. Zhang, *Phys. Rev. B* **99**, 155152 (2019).
- 18) R. Soto-Garrido, E. Muñoz, and V. Juričić, *Phys. Rev. Research* **2**, 012043 (2020).
- 19) T. Amitani and Y. Nishida, *Ann. Phys.* **448**, 169181 (2023).
- 20) X. Zheng, Q. Gu, Y. Liu, B. Tong, J.-F. Zhang, C. Zhang, S. Jia, J. Feng, and R.-R. Du, *Natl. Sci. Rev.* **9**, nwab191 (2022).
- 21) H. Hamasaki, Y. Tokumoto, and K. Edagawa, *Appl. Phys. Lett.* **110**, 092105 (2017).
- 22) H. Hamasaki, Y. Tokumoto, and K. Edagawa, *J. Phys. Soc. Jpn.* **89**, 023703 (2020).
- 23) C.-X. Liu, X.-L. Qi, H. Zhang, X. Dai, Z. Fang, and S.-C. Zhang, *Phys. Rev. B* **82**, 045122 (2010).
- 24) K.-I. Imura, M. Okamoto, Y. Yoshimura, Y. Takane, and T. Ohtsuki, *Phys. Rev. B* **86**, 245436 (2012).
- 25) Y. Meir and N. S. Wingreen, *Phys. Rev. Lett.* **68**, 2512 (1992).
- 26) S. Datta, *Quantum Transport: Atom to Transistor* (Cambridge University Press, Cambridge, 2005) Chap. 9.
- 27) The estimated energy gap is smaller than the bulk energy gap E_g (see Sect. 2). This is ascribed to the gap edge smearing due to finite size effects.
- 28) K. Nomura and N. Nagaosa, *Phys. Rev. Lett.* **106**, 166802 (2011).
- 29) K. Nomura, S. Ryu, A. Furusaki, and N. Nagaosa, *Phys. Rev. Lett.* **108**, 026802 (2012).
- 30) Roughly speaking, the energy gap induced in the spectrum of the helical surface states is nearly equal to m_{mag} , which we set $m_{\text{mag}}/m_{\parallel} = 1.2$. This is consistent with the behavior of T shown in Fig. 6. Indeed, the quantitative difference between the values of T in the presence and absence of the screw dislocations almost vanishes when $E_F/m_{\parallel} \gtrsim 1.2$.